Insight into One-Electron Oxidation of the {Fe(NO)(2)}(9) Dinitrosyl Iron Complex (DNIC): Aminyl Radical Stabilized by [Fe(NO)(2)] Motif

ARTICLE *in* INORGANIC CHEMISTRY · JANUARY 2013

Impact Factor: 4.76 · DOI: 10.1021/ic302537d · Source: PubMed

Inorganic Chemistry

Article

pubs.acs.org/IC

Insight into One-Electron Oxidation of the $\{Fe(NO)_2\}^9$ Dinitrosyl Iron Complex (DNIC): Aminyl Radical Stabilized by $[Fe(NO)_2]$ Motif

Chih-Chin Tsou,[†] Fu-Te Tsai,[†] Huang-Yeh Chen,[‡] I-Jui Hsu,*[,‡] and Wen-Feng Liaw*[,†]

[†]Department of Chemistry, National Tsing Hua University, Hsinchu, 30013, Taiwan

[‡]Department of Molecular Science and Engineering, National Taipei University of Technology, Taipei 10608 Taiwan

Supporting Information

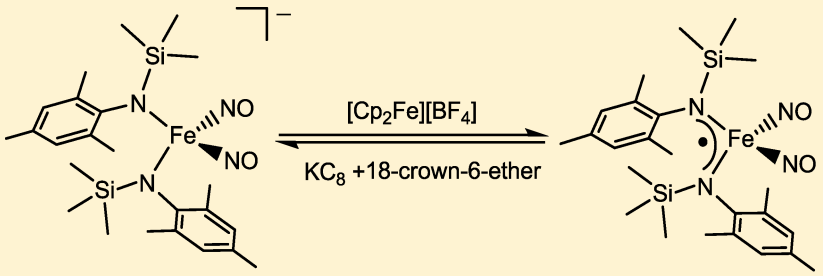

ABSTRACT: A reversible redox reaction ($\{Fe(NO)_2\}^9$ DNIC $[(NO)_2Fe(N(Mes)(TMS))_2]^-$ (**4**) ⇄ oxidized-form DNIC $[(NO)_2Fe(N(Mes)(TMS))_2]$ (**5**) (Mes = mesityl, TMS = trimethylsilane)), characterized by IR, UV−vis, $^1H/^{15}N$ NMR, SQUID, XAS, single-crystal X-ray structure, and DFT calculation, was demonstrated. The electronic structure of the oxidized-form DNIC **5** (S_{total} = 0) may be best described as the delocalized aminyl radical $[(N(Mes)(TMS))_2]_2^{-\bullet}$ stabilized by the electron-deficient $\{Fe^{III}(NO^-)_2\}^9$ motif, that is, substantial spin is delocalized onto the $[(N(Mes)(TMS))_2]_2^{-\bullet}$ such that the highly covalent dinitrosyl iron core (DNIC) is preserved. In addition to IR, EPR ($g \approx 2.03$ for $\{Fe(NO)_2\}^9$), single-crystal X-ray structure (Fe−N(O) and N−O bond distances), and Fe K-edge pre-edge energy (7113.1−7113.3 eV for $\{Fe(NO)_2\}^{10}$ vs 7113.4−7113.9 eV for $\{Fe(NO)_2\}^9$), the ^{15}N NMR spectrum of $[Fe(^{15}NO)_2]$ was also explored to serve as an efficient tool to characterize and discriminate $\{Fe(NO)_2\}^9$ (δ 23.1−76.1 ppm) and $\{Fe(NO)_2\}^{10}$ (δ −7.8−25.0 ppm) DNICs. To the best of our knowledge, DNIC **5** is the first structurally characterized tetrahedral DNIC formulated as covalent−delocalized $[\{Fe^{III}(NO^-)_2\}^9-[N(Mes)(TMS)]_2^{-\bullet}]$. This result may explain why all tetrahedral DNICs containing monodentate-coordinate ligands isolated and characterized nowadays are confined in the $\{Fe(NO)_2\}^9$ and $\{Fe(NO)_2\}^{10}$ DNICs in chemistry and biology.

INTRODUCTION

Dinitrosyl iron complexes (DNICs, Chart 1A), a possible form for storage and transport of NO, have been known to convey versatile physiological functions, such as vasodilation, inhibition of platelet aggregation, activation/inhibition of gene expression, and induction of anit/pro-apoptosis.[1] In chemistry, DNICs have also been demonstrated to exert S-nitrosylation, N-nitrosylation, nitrite activation, and phenol nitration.[2] According to Enemark and Feltham notation,[3] tetrahedral DNICs can be classified into the EPR-active, anionic/neutral/cationic $\{Fe(NO)_2\}^9$ DNICs as well as the EPR-silent, dianionic/anionic/neutral $\{Fe(NO)_2\}^{10}$ DNICs.[4] On the basis of EPR, X-ray absorption spectroscopy, Mössbauer, and DFT computation,[5] the electronic structure of $\{Fe(NO)_2\}^9$ DNICs (S_{total} = 1/2) with a characteristic EPR signal g value of ∼2.03 has been considered as high-spin Fe^{III} (S = 5/2) antiferromagnetically coupled to two triplet NO^- (S = 2) ligands (or a resonance hybrid consisting of the above-mentioned electronic structure and high-spin Fe^{II} (S = 2) antiferromagnetically coupled to an overall quartet $^4(NO)_2^-$ (S = 3/2)), in comparison with high-spin Fe^{II} (S = 2) antiferromagnetically coupled to two triplet NO^- (S = 2) in the $\{Fe(NO)_2\}^{10}$ DNICs. Can the tetrahedral $\{Fe(NO)_2\}^8$ DNICs be isolated? This question initiated the experiments reported here.

Recently, the six-coordinate *trans-syn*-$[Fe(TPP)(NO)_2]$ (TPP = *meso*-tetra-*m*-tolyl-porphinato), *trans-syn*-$[Fe(F_8)(NO)_2]$ (F_8 = tetraphenylporphinato), and *trans-syn*-$[Fe(TmPP)(NO)_2]$ (TmPP = tetrakis(2,6-difluorophenyl)-porphinato) were reported as unstable $\{Fe(NO)_2\}^8$ species (Chart 1B).[6] These six-coordinate $\{Fe(NO)_2\}^8$ DNICs could be prepared from stable $\{Fe(NO)\}^7$ mononitrosyl iron complexes (MNICs) and $NO_{(g)}$ at −80 °C but converting back to the original MNICs at ambient temperature. $\{Fe(NO)_2\}^8$ $[Fe(CN)_4(NO)_2]^{2-}$ was also proposed (Chart 1C).[7] In the reaction of $\{Fe(NO)\}^7$ $[(NO)Fe(SPh)_3]^-$ and $[NO]^+$ yielding $[(NO)_2Fe(\mu\text{-}SPh)]_2$, the intermediate $\{Fe(NO)_2\}^8$ $[(NO)_2Fe(SPh)_2]$ was proposed.[8] In biology, the protein-bound nonheme $\{Fe(NO)_2\}^8$ DNIC was considered as one of the products in the nitrosylation of *E. coli* ferric uptake

Received: November 20, 2012
Published: January 14, 2013

dx.doi.org/10.1021/ic302537d | *Inorg. Chem.* 2013, 52, 1631−1639

Chart 1. Structures of Four- and Six-Coordinate DNICs

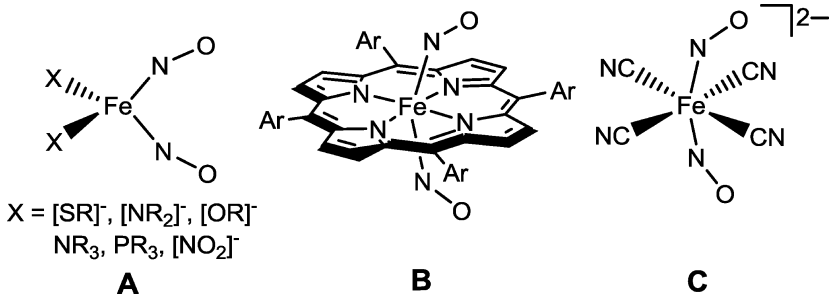

regulation protein (Fur).[9] In this manuscript, a reversible redox reaction ($\{Fe(NO)_2\}^9$ DNIC $[(NO)_2Fe(N(Mes)(TMS))_2]^-$ (**4**) ⇄ oxidized-form DNIC $[(NO)_2Fe(N(Mes)(TMS))_2]$ (**5**) (Mes = mesityl, TMS = trimethylsilane)) was demonstrated. In transition-metal−amido chemistry, amido ligands coordinated to the metal center have recently been demonstrated to bear noninnocent property, that is, $[M^{n+}-(NR_2)^-] \leftrightarrow [M^{(n-1)+}-(NR_2)^\bullet]$ ($(NR_2)^\bullet$ = aminyl radical), although transition-metal complexes $[M^{(n-1)+}-(NR_2)^\bullet]$ with the spin density predominantly localized at the nitrogen center are rare.[10] To the best of our knowledge, DNIC **5** obtained from one-electron oxidation of $\{Fe(NO)_2\}^9$ DNIC **4** is the first structurally characterized DNIC formulated as covalent-delocalized $[\{Fe^{III}(NO^-)_2\}^9-[N(Mes)(TMS)]_2^{-\bullet}]$, identified by IR, UV−vis, $^1H/^{15}N$ NMR, SQUID, X-ray absorption spectroscopy (XAS), single-crystal X-ray diffraction, and DFT calculation. Additionally, the ^{15}N NMR spectrum of $[Fe(^{15}NO)_2]$ was also explored to serve as an efficient tool to characterize and discriminate $\{Fe(NO)_2\}^9/\{Fe(NO)_2\}^{10}$ DNICs and $[\{Fe(NO)_2\}^9-\{Fe(NO)_2\}^9]/[\{Fe(NO)_2\}^{10}-\{Fe(NO)_2\}^{10}]$ dinuclear DNICs.

RESULTS AND DISCUSSION

Addition of 2 equiv of KNR_2 into toluene−THF solution of $[(NO)_2FeI_2]^-$ (**1**) at −78 °C yielded the thermally stable complex $[(NO)_2Fe(NR_2)_2]^-$ (NR_2 = NPh_2 (**2**), $N(TMS)_2$ (**3**), N(Mes)(TMS) (**4**) (Mes = mesityl, TMS = trimethylsilane)) (Figure 1a and Supporting Information Figures S1 ans S2). The mean Fe−N(O) and N−O bond lengths (Fe−N(O) = 1.691(4), 1.697(7), 1.700(3) Å and N−O = 1.171(4), 1.175(8), 1.186(3) Å for **2**, **3**, and **4**, respectively) fall in the range of 1.661(4)−1.695(3) Å (Fe−N(O)) and 1.160(6)−1.178(3) Å (N−O) observed in the $\{Fe(NO)_2\}^9$ DNICs.[4c] In comparison with the IR ν_{NO} spectrum (1774, 1712 cm^{-1}) of the $\{Fe(NO)_2\}^9$ DNIC $[(NO)_2Fe(Im\text{-}H)_2]^-$ (Im-H = imidazolate),[11] IR ν_{NO} spectra of **2** (1727, 1672 cm^{-1}), **3** (1711, 1650 cm^{-1}), and **4** (1707, 1652 cm^{-1}) provide the opportunity to directly probe the binding affinity of the $\{Fe(NO)_2\}^9$ motif toward the N-containing coordinate ligands as investigated in the previous study,[5b] that is, in the order of $[Im\text{-}H]^- < [NPh_2]^- < [N(TMS)_2]^- \approx [N(Mes)(TMS)]^-$. As shown in Figure 2, complex **4** exhibits a 9-line EPR signal with g_{av} = 2.015 ($A_{N(NO)}$ = 3.64 G and $A_{N(amido)}$ = 3.64 G) at 298 K (a 13-line EPR signal with g_{av} = 2.019 ($A_{N(NO)}$ = 2.40 G, $A_{N(amido)}$ = 4.64 G) for **2** (Supporting Information Figure S3) and a 19-line EPR signal with g_{av} =2.020 ($A_{N(NO)}$ = 2.45 G, $A_{N(amido)}$ = 3.75 G) for **3** (Supporting Information Figure S4)), the characteristic signal of tetrahedral $\{Fe(NO)_2\}^9$ DNICs $[(NO)_2FeX_2]^-$ (X = thiolate, imidazolate, phenoxide).[5b,11,12] The EPR splitting lines of DNICs **2**, **3**, and **4** can be rationalized by the unpaired electron coupling with nitrogens of the amido ligands and the nitrosyl groups, as observed in the previous study.[12d] The temperature-independent effective magnetic moment (μ_{eff}) of complex **4** decreases from 1.924 μ_B at 300 K to 1.714 μ_B at 2 K (Curie law fitting of $\chi_M T$ vs T plot gives g = 2.049, θ = −0.146 ± 0.005 K, TIP = (226 ± 1.3) × 10^{-6} cm^3 mol^{-1}, and R^2 = 0.993 (Supporting Information Figure S5)), consistent with the S = 1/2 ground state.

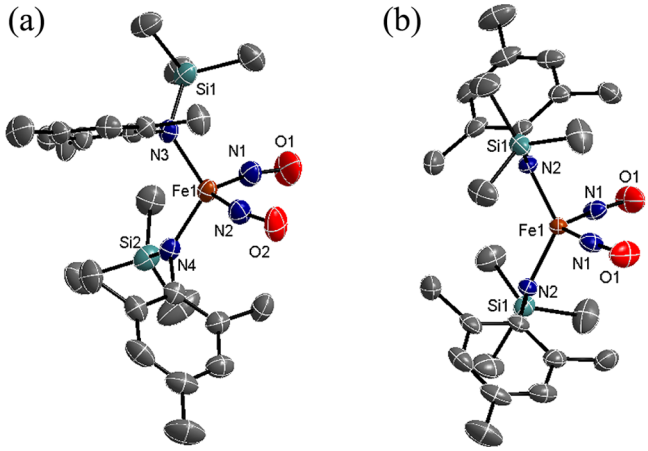

Figure 1. ORTEP drawing and labeling schemes of (a) $[(NO)_2Fe(N(Mes)(TMS))_2]^-$ (**4**) in $[(THF)_2$-K-18-crown-6-ether$)]^+$ salt and (b) $[(NO)_2Fe(N(Mes)(TMS))_2]$ (**5**) with thermal ellipsoids drawn at 50% probability. Selected bond distances (Angstroms) and angles (degrees): Fe(1)−N(1) 1.698(3), Fe(1)−N(2) 1.701(3), Fe(1)−N(3) 1.983(2), Fe(1)−N(4) 1.992(3), N(1)−O(1) 1.180(3), N(2)−O(2) 1.191(3), N(3)−Si(1) 1.718(3), N(4)−Si(2) 1.717(3), N(1)−Fe(1)−N(2) 105.8(1), N(3)−Fe(1)−N(4) 117.0(1), Fe(1)−N(1)−O(1) 162.2(3), Fe(1)−N(2)−O(2) 154.6(3) for **4**; Fe(1)−N(1) 1.662(3), Fe(1)−N(2) 1.893(2), N(1)−O(1) 1.163(3), N(2)−Si(1) 1.759(3), N(1)−Fe(1)−N(1A) 112.1 (2), N(2)−Fe(1)−N(2A) 128.9(1), Fe(1)−N(1)−O(1) 161.9(3) for **5**.

In contrast to the free ligand [K][N(Mes)(TMS)] displaying irreversible oxidation (E_{ox} = −0.89 V (THF)), the electrochemistry of complex **4**, measured in THF with 0.2 M $[n\text{-}Bu_4N][PF_6]$ as supporting electrolyte at room temperature (scan rate 100 mV/s), reveals a reversible oxidation−reduction couple at −0.81 V (vs Cp_2Fe^+/Cp_2Fe; Figure 3). As shown in Scheme 1a, DNIC **4** reacted on time of mixing with 1 equiv of $[Cp_2Fe][BF_4]$ in THF to yield the neutral, deep-blue $[(NO)_2Fe(N(Mes)(TMS))_2]$ (**5**). DNIC **5** is thermally stable in the solid state and THF solution at −20 °C. In a similar fashion, oxidation of complexes **2** and **3** yielded the proposed thermally unstable $[(NO)_2Fe(NPh_2)_2]$ (ν_{NO} = 1768, 1711 cm^{-1}) and $[(NO)_2Fe(N(TMS)_2)_2]$ (ν_{NO} = 1774, 1708 cm^{-1}), respectively, based on IR ν_{NO} spectra and cyclic voltammo-

dx.doi.org/10.1021/ic302537d | Inorg. Chem. 2013, 52, 1631−1639

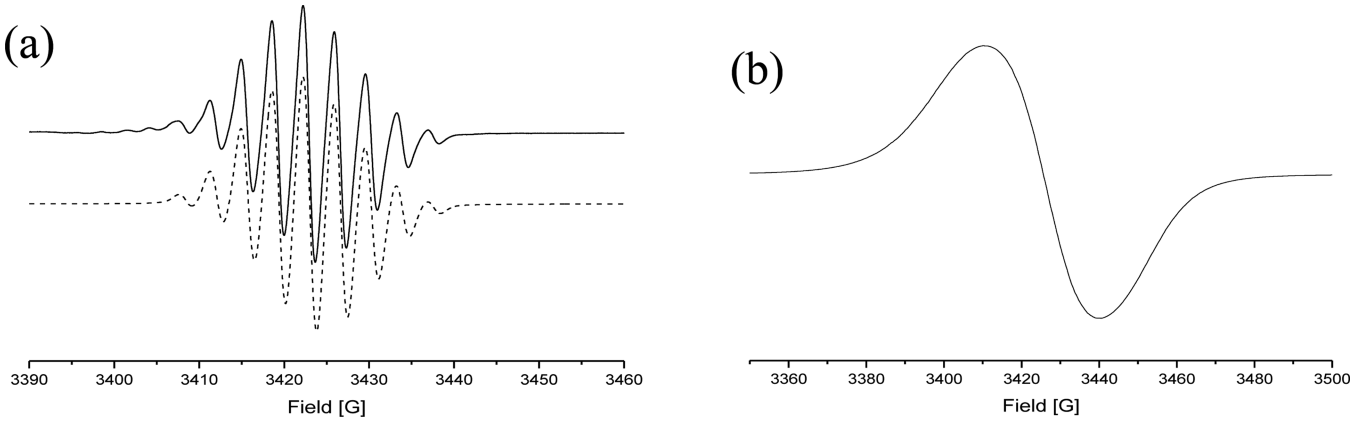

Figure 2. EPR spectra of complex **4** in THF (a) at 298 K (solid line) and the simulation curve (dash line) with g_{av} = 2.015 and $A_{N(NO)}$ = 3.64 G, $A_{N(amido)}$ = 3.64 G and (b) at 77 K (g_1 = 2.022, g_2 = 2.013, g_3 = 2.005).

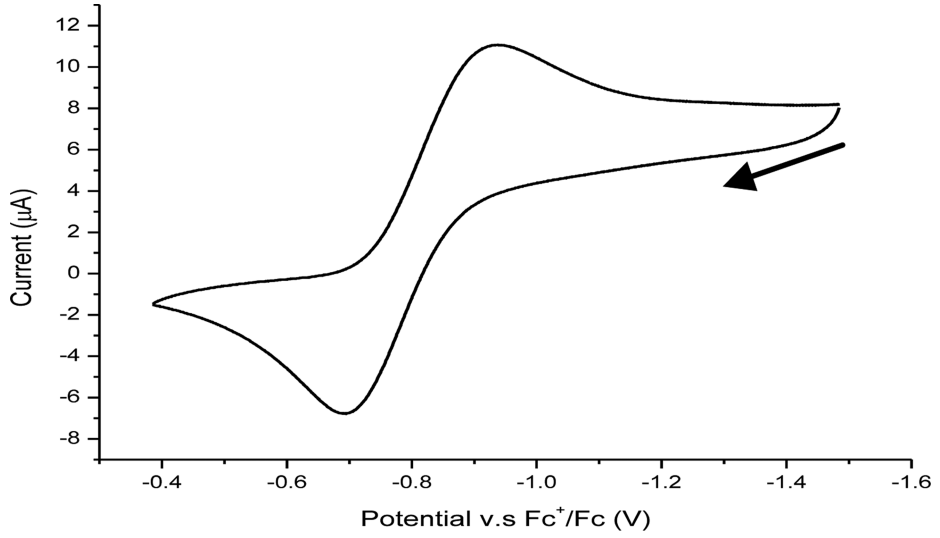

Figure 3. Cyclic voltammogram of DNIC **4** in 20 mM THF with 0.2 M [n-Bu_4N][PF_6] as the supporting electrolyte at room temperature and scan rate of 100 mV/s showing a reversible redox wave with $E_{1/2}$ = −0.813 V (vs Cp_2Fe^+/Cp_2Fe) and i_{pa}/i_{pc} = 0.96.

Scheme 1. Reversible Redox Transformation between $\{Fe(NO)_2\}^9$ 4 and [$\{Fe(NO)_2\}^9$-Delocalized Aminyl Radical] 5 (L = [N(Mes)(TMS)])

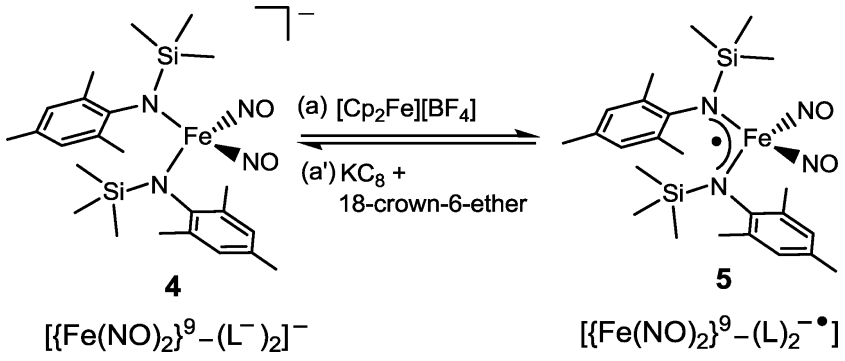

grams (Supporting Information Figure S6). In a comparison of complex **4** displaying absorptions at 380, 442 (sh), and 634 nm, the UV−vis spectrum of complex **5** displays intense absorptions at 624, 664 (sh), and 942 nm in THF (Supporting Information Figure S7). The higher energy ν_{NO} bands of complex **5** (1786, 1733 cm^{-1}) shifted by $\Delta\nu_{NO} \approx 80$ cm^{-1} from those of complex **4**, implicating a variation in the electronic structure of the [$Fe(N(Mes)(TMS))_2$] motif, in contrast to the significant difference in $\Delta\nu_{NO}$ value ($\Delta\nu_{NO} \approx 100-146$ cm^{-1};[4,5f] Figure 4 and Supporting Information Table S1) deriving from iron-based oxidation of $\{Fe(NO)_2\}^{10}$ DNICs producing $\{Fe(NO)_2\}^9$ DNICs.[5d−f] Figure 1b displays the ellipsoid plot of complex **5**. The local geometry of iron in complexes **4** and **5** is a distorted tetrahedron with $N_{(NO)}-Fe-N_{(NO)}$ and $N_{(NR2)}-Fe-N_{(NR2)}$ bond angles of 112.1(2)° and 128.9(1)° for **5** (vs 105.8(1)° and 117.0(1)° for **4**). The average Fe−N(O) and

dx.doi.org/10.1021/ic302537d | Inorg. Chem. 2013, 52, 1631−1639

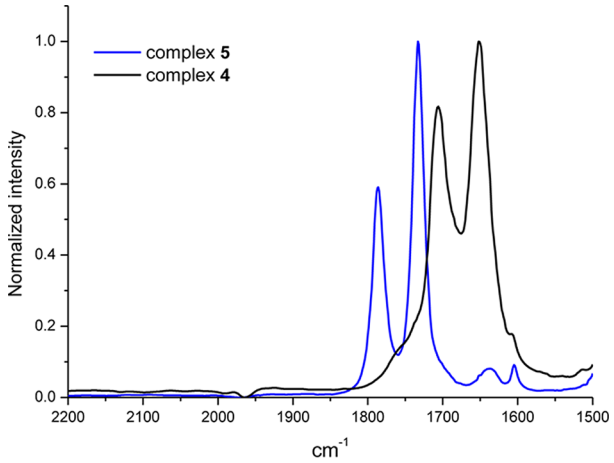

Figure 4. IR spectra of complexes **4** (black) and **5** (blue) in THF.

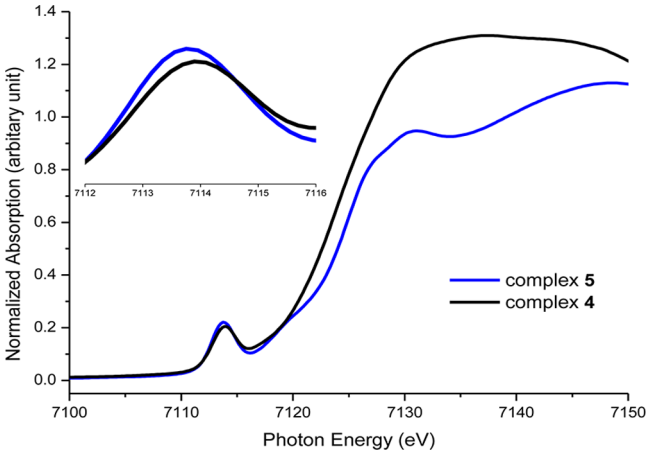

Figure 5. Fe K-edge spectra of complexes **4** (black) and **5** (blue), and the pre-edge absorption spectra are enlarged in the inset.

N−O bond distances of **5** fall within the range of $\{Fe(NO)_2\}^9$ DNICs observed in the previous study.[4c] It is noticed that the shortening in the average $Fe-N_{(NR2)}$ bond length from 1.988(3) Å for **4** to 1.893(2) Å for **5** is consistent with the shortening from the Cu^I−amido bond length of 2.0019(18) Å to the Cu^I−aminyl radical bond length of 1.906(2) Å.[10g] The increase ($\Delta_{N-Si} \approx 0.04$ Å) of N−Si bond distance (1.718(3) Å for **4** vs 1.759(3) Å for **5**) also implicates that oxidation occurs on the nitrogens of the amido ligands. On the basis of CV, IR, and the single-crystal X-ray structure ($Fe-N_{(NR2)}$ and N−Si bond lengths), oxidation of DNIC **4** converting it to DNIC **5** is, presumably, a ligand-centered oxidation from Fe−amido (**4**) to Fe−aminyl radical (**5**).

During the reversible redox transformation DNIC **4** ⇄ DNIC **5**, complex **5** stabilized by [$\{Fe(NO)_2\}^9$−aminyl radical] electronic configuration implicates that the iron center of DNICs is tailored to minimize the electronic changes, modulated by the redox-active Fe center and the [N(Mes)-(TMS)]-coordinate ligands, to preserve the $\{Fe(NO)_2\}^9$ electronic core. This point has received further support in the study of XAS of DNICs **4** and **5**. The Fe K-edge pre-edge energy derived from the 1s → 3d transition in a distorted T_d environment of the Fe center is 7113.9 and 7113.7 eV for **4** and **5**, respectively, within the range of 7113.4−7113.8 eV for $\{Fe^{III}(NO^-)_2\}^9$ DNICs (7113.1−7113.3 eV for $\{Fe^{II}(NO^-)_2\}^{10}$ DNICs) (Figure 5 and Supporting Information Figure S8).[5b,f] This result suggests that oxidation of DNIC **4** mainly occurs on the [N(Mes)(TMS)]-coordinate ligands. As collected from this study, the ^{15}N NMR (^{15}NO) chemical shift of $\{Fe(NO)_2\}^{10}$ DNICs lies in the range of δ −7.8−25.0 ppm. It is noticed that the ^{15}N NMR spectrum of **5** at 298 K displays δ 62.3 (s) ppm (^{15}NO) in d_8-THF, within the range (δ 23.1−76.1 ppm (^{15}NO)) of $\{Fe(NO)_2\}^9$ DNICs summarized from this investigation (Table 1; Supporting Information Figure S9).[2a,13] The ^1H NMR spectrum of **5** at 298 K shows the chemical shift (δ 6.82 (4H, br s, Mes), 2.31 (18H, br s, 2,4,6-CH_3-Mes), and 0.17 ppm (18H, br s, $Si(CH_3)_3$ in d_8-toluene) for [N(Mes)(TMS)]-coordinate ligands) (Supporting Information Figure S10), compared to the sharp peaks (δ 6.88, 2.39, 2.25, 0.39 ppm) observed in $(THF)_2Mg[N(Mes)(TMS)]_2$.[14] The broad ^1H NMR peaks suggest that the singlet-ground-state DNIC **5** has a low-lying triplet excited state with small thermal population.[15] In order to estimate the singlet/triplet energy splitting ($\Delta_{S/T}$), the magnetic susceptibility measurement of powder sample of **5** was collected in the temperature range of 5−300 K at 0.5 T. The temperature-dependent effective magnetic moment in the solid state by SQUID decreases from 0.622 μ_B at 300 K to 0.326 μ_B at 5 K. Experimental data were fitted to the electronic structure [$\{Fe^{III}(NO^-)_2\}^9-(L)_2^{-\bullet}$] (L = [N(Mes)(TMS)]). The best fit with the g values for $\{Fe(NO)_2\}^9$ and $(L)_2^{-\bullet}$ fixed to 2.015 and 2.000, respectively, corresponds to ~97% [$\{Fe^{III}(NO^-)_2\}^9-(L)_2^{-\bullet}$] ($\Delta_{S/T}$ = 1840 ± 68 cm^{-1} with R^2 = 0.999 and TIP = (81.8 ± 0.4) × 10^{-6} cm^3 mol^{-1} (Supporting Information Figure S11). On the basis of IR, single-crystal X-ray structure, SQUID, Fe K-edge pre-edge energy, and $^1H/^{15}N$ NMR, the [$\{Fe^{III}(NO^-)_2\}^9-(L)_2^{-\bullet}$] ($S_{total}$ = 0) electronic structure is suggested for **5**, that is, substantial spin is delocalized onto the $[(N(Mes)(TMS))_2]_2^{-\bullet}$ such that the highly covalent dinitrosyl iron core is preserved. These results may lend support to the electronic structure of the previously proposed $\{Fe(NO)_2\}^8$ intermediate $[(^{15}NO)_2Fe-(DTC)_2]$ (^{15}N NMR δ 40.4 (s) ppm), which may be best described as [$\{Fe^{III}(NO^-)_2\}^9-(DTC)_2^{-\bullet}$] (DTC = S_2CNMe_2).[2a] Reversibly, formation of **4** was observed upon addition of 1 equiv of KC_8 and 18-crown-6-ether to the THF solution of **5** at ambient temperature (Scheme 1a′), characterized by IR, UV−vis, and EPR spectroscopies. These results may explain why there is no tetrahedral $\{Fe(NO)_2\}^8$ DNIC isolated nowadays in chemistry and biology, due to the electron-deficient $\{Fe(NO)_2\}^9$ core.

The SOMO and HOMO of DNICs **4** and **5** based on the unrestricted DFT calculation with B3LYP* exchange functional are displayed in the Figure 6a (Supporting Information Figure S12) and 6b (Supporting Information Figure S13), respectively. The SOMO of **4** is mainly contributed from both ligands (41.4% 2p) along with the $\{Fe^{III}(NO^-)_2\}^9$ motif (8.6% $Fe_{dx^2-y^2}$ + 1.2% NO 2p). As one-electron oxidation of **4** yields **5**, the HOMO of **5**, close to the SOMO-1 of **4**, is composed of both ligands (30.9% 2p) and the $\{Fe^{III}(NO^-)_2\}^9$ motif (5.2% $Fe_{d_{xy}}$ + 17.8% NO 2p). The energy difference between the singlet and the triplet of DNIC **5** is ~1460 cm^{-1} (Supporting Information Table S2), consistent with fitting results of magnetic measurement. This result together with the equivalent $Fe-N_{(NR2)}$ bond distances suggest the interaction between $\{Fe^{III}(NO^-)_2\}^9$ and $[(L)_2^{-\bullet}]$ is best described as covalent delocalization in complex **5**.[15] According to TD-DFT calculation of **5**, the peak around 942 nm is assigned as the transition from the HOMO to the LUMO, indicating charge transfer is derived from aminyl ligands to the Fe site (Figure 7). It is noteworthy that the

dx.doi.org/10.1021/ic302537d | Inorg. Chem. 2013, 52, 1631−1639

Table 1. ^{15}N NMR Chemical Shift (^{15}NO) of $\{Fe(^{15}NO)_2\}^{9/10}$ DNICs and $[\{Fe(^{15}NO)_2\}^{9/10}$-$\{Fe(^{15}NO)_2\}^{9/10}]$ Dinuclear DNICs[a]

		δ (^{15}N)			
EF notation	complex	C_{2h} isomer	C_{2v} isomer	solvent	ref
$[\{Fe(NO)_2\}^9]_2$	$[Fe(\mu\text{-}StBu)(^{15}NO)_2]_2$	38.8 (s)	31.1, 37.1 (d, J = 3.0)	d_8-toluene	2a
		41.7 (s)	34.6, 40.3 (s)	d_8-THF	13b
$[\{Fe(NO)_2\}^9]_2$	$[Fe(\mu\text{-S-NAP})(^{15}NO)_2]_2$	42.6 (s)	41.3, 36.7 (s)	d_6-DMSO	2a
		40.7, 42.5 (s)	34.6, 40.3 (s)	d_8-THF	
$[\{Fe(NO)_2\}^9]_2$	$[Fe(\mu\text{-}SiPr)(^{15}NO)_2]_2$	30.2 (s)	26.7, 35.7 (d, J = 2.6)	d_8-toluene	13
$[\{Fe(NO)_2\}^9]_2$	$[Fe(\mu\text{-SEt})(^{15}NO)_2]_2$	31.4 (s)	25.0, 36.1 (d, J = 3.0)	d_8-toluene	13b
		34.4 (s)	28.8, 39.2 (s)	d_8-THF	this work
		35.0 (s)	29.6, 39.5 (s)	CD_3CN	
$[\{Fe(NO)_2\}^9]_2$	$[Fe(\mu\text{-SMe})(^{15}NO)_2]_2$	30.5 (s)	23.1, 36.2 (d, J = 2.8)	d_8-toluene	13
$[\{Fe(NO)_2\}^9]_2$	$[Fe(\mu\text{-SPh})(^{15}NO)_2]_2$	34.2 (s)	25.9, 39.4 (d, J = 3.0)	d_8-toluene	13b
$[\{Fe(NO)_2\}^9]_2$	$[Na]_2[Fe_2S_2(^{15}NO)_4]$	37.8 (s)		D_2O	13b
$[\{Fe(NO)_2\}^9]_3$	$[PPN][Fe_4S_3(^{15}NO)_7]$	36.0, 76.1 (d, J = 4.3 Hz)		CD_2Cl_2	13a
$[\{Fe(NO)_2\}^9]_3$	$[PPN][Fe_4Se_3(^{15}NO)_7]$	29.5, 74.9 (d, J = 4.1 Hz)		CD_2Cl_2	13a
$[\{Fe(NO)_2\}^9]$	complex **5**	60.9 (s)		d_8-toluene	this work
		62.3 (s)		d_8-THF	
$[\{Fe(NO)_2\}^9]$	proposed $[(DTC)_2^{-\bullet}$-$Fe(^{15}NO)_2]$[b]	40.3 (s)		d_6-DMSO	2a
		40.4 (s)		d_8-THF	
$[\{Fe(NO)_2\}^{10}]$	$[(spartein)Fe(^{15}NO)_2]$	0.27 (s), −7.77 (s)		d_8-toluene	this work
		1.55 (d, J = 18.6 Hz), −6.76 (d, J = 16.7 Hz)		d_8-THF	
		3.87 (s), −4.10 (s)		CD_3CN	
$[\{Fe(NO)_2\}^{10}]$	$[(TMEDA)Fe(^{15}NO)_2]$	−6.48 (s)		d_8-THF	this work
$[\{Fe(NO)_2\}^{10}]$	$[(EtS)_2Fe(^{15}NO)_2]^{2-}$[c]	18.2 (s)		d_8-THF	this work
		19.2 (s)		CD_3CN	
$[\{Fe(NO)_2\}^{10}]_2$	$[Fe(\mu\text{-SEt})(^{15}NO)_2]_2^{2-}$[c]	24.3 (s)		CD_3CN	this work
$[\{Fe(NO)_2\}^{10}]_2$	$[PPN]_2[Fe(\mu\text{-}StBu)(^{15}NO)_2]_2$	25.0 (s)		CD_3CN	this work

[a]The angles of M−N−O in these $\{Fe(NO)_2\}^{9/10}$ DNICs and dinuclear DNICs lie in the range of 159−176°. Although the ^{15}N NMR chemical shift strongly depends on the linear or bent M−N−O,[13c] the difference of ^{15}N NMR chemical shifts between $\{Fe(NO)_2\}^9$ and $\{Fe(NO)_2\}^{10}$ DNICs may be mainly attributed to the different oxidation state of the $[Fe(NO)_2]$ core. [b]DTC = dimethyldithiocarbamate. [c]Complexes with $[K\text{-}18\text{-crown-}6\text{-ether}]_2^{2+}$ cations.

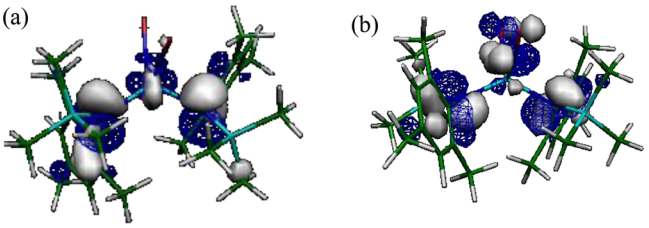

Figure 6. SOMO and HOMO of DNICs (a) **4** and (b) **5**, respectively.

frontier MOs of **4** are similar to those of $[(NO)_2Fe(EPh)_2]^-$ (E = S, O) obtained from the previous study.[5b] This computation supports the fact that oxidation of $\{Fe(NO)_2\}^9$ $[(NO)_2Fe(EPh)_2]^-$ dominantly occurs from S/O-coordinate ligands, rationalizing one-electron oxidation of $[(NO)_2Fe(SR)_2]^-$ yielding $[(NO)_2Fe(\mu\text{-SR})]_2$ and disulfide (Supporting Information Scheme S1).

CONCLUSION AND COMMENTS

In contrast to the free ligand [K][N(Mes)(TMS)] exhibiting irreversible oxidation in the cyclic voltammogram, the redox interconversion DNIC **4** ⇄ DNIC **5** is reversible. The electronic structure of the one-electron-oxidized form, DNIC **5**, characterized by a detailed analysis of IR, UV−vis, ^{1}H/^{15}N NMR, SQUID, XAS, single-crystal X-ray structure, and DFT calculation, is best described as $[\{Fe^{III}(NO^-)_2\}^9-(L)_2^{-\bullet}]$ (S_{total} = 0) instead of $[\{Fe(NO)_2\}^8-(L^-)_2]$, that is, the redox couple at −0.81 V is mainly due to the ligand-based oxidation−reduction as opposed to the $\{Fe(NO)_2\}^8/\{Fe(NO)_2\}^9$ couple. It may be attributed to the delocalized aminyl radical being stabilized by an electron-deficient $\{Fe(NO)_2\}^9$ fragment. One could also envision six-coordinate $\{Fe(NO)_2\}^8$ complexes to be generally unstable, as they have a suitable decomposition pathway that leads to generation of very stable $\{Fe(NO)\}^7$ complexes and release of NO.[2a,6,7] That is, $\{Fe(NO)_2\}^8$ complexes do not seem to form easily, at least not as stable species at room temperature. In the other direction, these results also rationalize why reaction of four-coordinate $\{Fe(NO)\}^7$ mononitrosyl iron complexes (MNICs) and NO yielding $\{Fe(NO)_2\}^8$ DNICs has never been observed.[8] In addition to EPR, IR, NRVS,[16] Fe K-edge pre-edge energy, and single-crystal X-ray structure, the ^{15}N NMR (^{15}NO) chemical shift of $\{Fe(^{15}NO)_2\}^{9/10}$ DNICs was demonstrated to serve as an efficient tool to characterize and discriminate $\{Fe(NO)_2\}^9$ (δ 23.1−76.1 ppm) DNICs and $\{Fe(NO)_2\}^{10}$ (δ −7.8−25.0 ppm) DNICs. Study of the electronic structures of the redox forms DNIC **4** ⇄ DNIC **5** may point the way to understanding why all tetrahedral DNICs containing monodentate-coordinate ligands isolated and characterized nowadays are confined in the $\{Fe(NO)_2\}^9$ and $\{Fe(NO)_2\}^{10}$ DNICs in chemistry and biological systems[1−5,9,12a−c] and gaining insight into the feature of DNICs under oxidative stress,[1e,17] albeit the $\{Fe(NO)_3\}^{10}$ TNICs and $\{Fe(NO)\}^{6/7/8}$ MNICs have been isolated.[18]

dx.doi.org/10.1021/ic302537d | Inorg. Chem. 2013, 52, 1631−1639

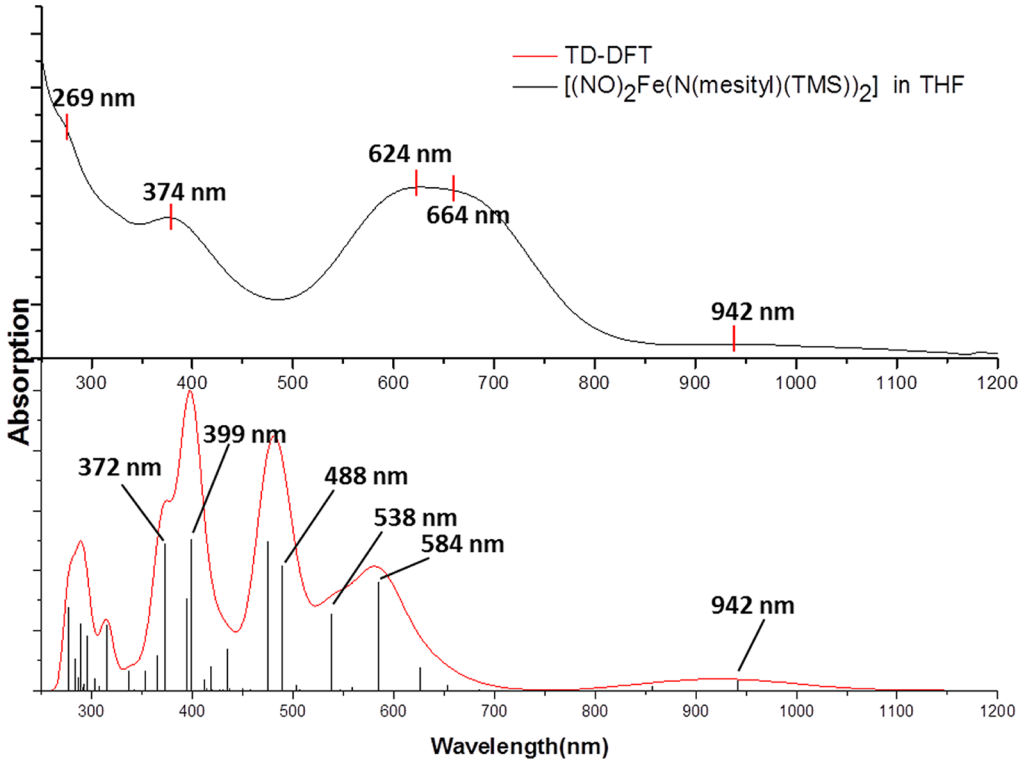

Figure 7. Comparison of UV−vis−NIR spectra of complex **5** between the experimental (top) and the calculated results (down). TD-DFT calculation peaks have been convoluted by Gaussian profile shape with fwhm = 0.1 eV. In order to compare both experimental and calculated spectra, a 0.32 eV shift was applied to the calculated spectrum.

EXPERIMENTAL SECTION

Materials. Manipulations, reactions, and transfers were conducted under nitrogen according to Schlenk techniques or in a glovebox (nitrogen gas). Solvents were distilled under nitrogen from appropriate drying agents (MeOH from I_2 and Mg; MeCN from CaH_2; hexane, toluene, diethyl ether, and tetrahydrofuran (THF) from sodium and benzophenone) and stored in dried, N_2-filled flasks over 4 Å molecular sieves. Nitrogen was purged through these solvents before use. Solvent was transferred to the reaction vessel via stainless cannula under a positive pressure of N_2. Reagents $[K][N(TMS)_2]$ (TMS = trimethylsilane) (95%), $HNPh_2$, $[Cp_2Fe][BF_4]$, diglyme, CD_3CN, d_8-THF, d_8-toluene (Sigma-Aldrich), 30% KH (Lancaster), 18-crown-6-ether (TCI), KI (SHOWA), and $Na^{15}NO_2$ (ISOTEC) were used as received. Compounds [HN(mesityl)(TMS)], $[Fe(CO)_2(NO)_2]$, $[PPN][(NO)_2Fe(SPh)_2]$, and $[PPN][(NO)_2Fe(SEt)_2]$ were synthesized by published procedures.[8,14,19] Infrared spectra of the ν_{NO} stretching frequencies were recorded on a Perkin Elmer model spectrum One B spectrometer with sealed solution cells (0.1 mm, CaF_2 windows). UV−vis spectra were recorded on a Jasco V-570 spectrometer. ^1H and ^{15}N NMR spectra were acquired on a VARIAN UNITY INOVA 500 NMR spectrometer. ^{15}N NMR spectra were recorded at 50.671 MHz, and 1024 transients were acquired with a 2 s delay time. Chemical shifts (δ) of ^{15}N NMR are relative to neat 1 M $Na^{15}NO_2$ in D_2O (δ 232 ppm) as the external standard.[2a,13c] Analyses of carbon, hydrogen, and nitrogen were obtained with a CHN analyzer (Heraeus).

General Procedure for Synthesis of $[K][NR_2]$ (NR_2 = NPh_2 and N(mesityl)(TMS)). To a stirred suspension of KH (11 mmol, 0.4412 g) in THF (10 mL) at 0 °C, $HNPh_2$ (10 mmol, 1.6922 g) (or [HN(mesityl)(TMS)] (10 mmol, 2.0739 g)) in THF (20 mL) was added dropwise. The reaction was allowed to stir at room temperature until cessation of $H_{2(g)}$ production. The resulting mixture was filtered through Celite to remove the insoluble solid, and then hexane was added to result in precipitation of the pale-yellow solid $[K][NPh_2]$ (yield 2.010 g, 97%) (white solid [K][N(mesityl)(TMS)] (yield 2.331 g, 95%)). Compound $[K][NPh_2]$: ^1H NMR (500 MHz, d_8-THF, 25 °C): δ 6.85 (8H, m, *m,o*-C*H*), 6.16 (2H, m, *p*-C*H*). IR: 3060 m, 3043 m, 3010 w, 2980 w, 1592 s, 1571 s, 1520 m, 1471 s, 1438 w, 1419 w, 1357 s, 1345 s, 1320 s, 1256 w, 1170 s, 1147 m, 1076 w, 1025 w, 989 m, 876 w, 859 w, 800 w, 749 s, 692 s, 523 m, 502 w cm^{-1} (KBr). Anal. Calcd for $C_{12}H_{10}NK$: C, 69.52; H, 4.86; N, 6.76. Found: C, 68.51; H, 5.18; N, 6.45. Compound [K][N(mesityl)(TMS)]: ^1H NMR (500 MHz, d_8-toluene, 25 °C): δ 6.78 (2H, s, mesitylene), 2.18 (3H, s, 4-CH_3-mesitylene), 2.15 (6H, s, 2,6-CH_3-mesitylene), 0.10 ppm (3H, s, Si(CH_3)$_3$). IR: 2944 s, 2910 s, 2866 m, 1598 m, 1471 s, 1432 s, 1367 m, 1343 s, 1306 m, 1251 s, 1230 s, 1157 w, 997 m, 984 m, 943 w, 895 s, 838 s, 761 w, 734 w, 661 m cm^{-1} (KBr). Anal. Calcd for $C_{12}H_{20}NKSi$: C, 58.71; H, 8.21; N, 5.71. Found: C, 58.58; H, 8.92; N, 5.58.

Preparation of $[(THF)_2$-K-18-crown-6-ether$][(NO)_2FeI_2]$ (1).[20] KI (1.8260 g, 11.0 mmol), I_2 (1.2690 g, 5.0 mmol), and 18-crown-6-ether (2.6432 g, 10.0 mmol) were loaded into a Schlenk flask and dissolved in MeOH (30 mL). After stirring for 1 h, the reaction mixture was transferred to the freshly prepared MeOH solution of $[Fe(CO)_2(NO)_2]$ (10.0 mmol) in a dropwise manner at 0 °C. The reaction solution was then stirred at room temperature overnight. The resulting greenish-brown solution was dried under reduced pressure. The crude solid was redissolved in THF−diethyl ether (30:15 mL) and filtered through Celite to remove the insoluble solid. Addition of hexane to the filtrate led to precipitation of complex $[(THF)_2$-K-18-crown-6-ether$][(NO)_2FeI_2]$ (**1**). Pure complex **1** (yield 5.802 g, 71%) was isolated after being washed three times by diethyl ether (30 mL). IR: 1765 s, 1713 s (ν_{NO}) cm^{-1} (THF). The ^{15}N-labeled complex **1** $[(THF)_2$-K-18-crown-6-ether$][(^{15}NO)_2FeI_2]$ was synthesized in the same manner by reaction of $[Fe(CO)_2(^{15}NO)_2]$,[2a] KI, I_2, and 18-crown-6-ether. IR: 1733 s, 1679 s (ν_{15NO}) cm^{-1} (THF).

Synthesis of $[(THF)_2$-K-18-crown-6-ether$][(NO)_2Fe(NPh_2)_2]$ (2). The THF (30 mL) solution of $KNPh_2$ (0.2073 g, 1.0 mmol) was added dropwise to the THF (10 mL) solution of complex **1** (0.4087 g, 0.5 mmol) at −78 °C. The reaction mixture was allowed to warm to ambient temperature and stirred for 3 h. The resulting purple mixture was filtered through Celite to remove the insoluble solid. The

dx.doi.org/10.1021/ic302537d | Inorg. Chem. 2013, 52, 1631−1639

solution was concentrated under reduced pressure, and then hexane (20 mL) was added to lead to precipitation of the purple solid [(THF)$_2$-K-18-crown-6-ether][(NO)$_2$Fe(NPh$_2$)$_2$] (**2**). KI byproduct was removed by extraction with diglyme. X-ray-quality crystals were obtained by layering the THF solution of complex **2** with hexane at ambient temperature for 1 week (yield 0.318 g, 71%). IR: 1727 s, 1672 s (ν_{NO}) cm^{-1} (THF). Absorption spectrum (THF) [nm, λ_{max} (M^{-1} cm^{-1}, ε)]: 270 (24 100), 315 (sh, 19 400), 380 (sh, 5300), 465 (sh, 3570), 516 (3630), 760 (sh, 2320). Anal. Calcd for $C_{44}H_{60}FeKN_4O_{10}$: C, 58.72; H, 6.72; N, 6.23. Found: C, 58.11; H, 6.59; N, 6.73.

Synthesis of [K-18-crown-6-ether)][(NO)$_2$Fe(N(TMS)$_2$)$_2$] (3) and [(THF)$_2$-K-18-crown-6-ether][(NO)$_2$Fe(N(mesityl)(TMS))$_2$] (4). The toluene (15 mL) solution of [K][N(TMS)$_2$] (0.2010 g, 1.0 mmol, 95%) (or [K][N(mesityl)(TMS)] (0.2455 g, 1.0 mmol)) was added dropwise to the THF−toluene (2:5 mL) solution of complex **1** (0.4087 g, 0.5 mmol) at −78 °C. The reaction mixture was allowed to warm to ambient temperature and stirred for 3 h. After the mixture solution was dried under vacuum, the crude solid was redissolved in diethyl ether. The resulting brown solution was filtered through Celite to remove the insoluble solid. Addition of hexane to the mixture solution led to precipitation of the brown solid [K-18-crown-6-ether][(NO)$_2$Fe(N(TMS)$_2$)$_2$] (**3**) and [(THF)$_2$-K-18-crown-6-ether][(NO)$_2$Fe(N(mesityl)(TMS))$_2$] (**4**), respectively. X-ray-quality crystals of complexes **3** and **4** were obtained by layering the diethyl ether solution of complex **3** (yield 0.2876 g, 78%) with hexane (or by layering the THF solution of complex **4** (yield 0.4015 g, 82%) with hexane) at −20 °C for 1 week. Complex **3**: IR: 1711 s, 1650 s (ν_{NO}) cm^{-1} (THF); 1709 s, 1644 s (ν_{NO}) cm^{-1} (Et$_2$O). Absorption spectrum (THF) [nm, λ_{max} (M^{-1} cm^{-1}, ε)]: 265 (sh, 6700), 318 (sh, 3500), 340 (sh, 3300), 495 (sh, 610), 630 (390). Anal. Calcd for $C_{24}H_{60}FeKN_4O_8Si_4$: C, 38.95; H, 8.17; N, 7.57. Found: C, 38.71; H, 8.50; N, 7.67. Complex **4**: IR: 1707 s, 1652 s (ν_{NO}) cm^{-1} (THF); 1703 s, 1649 s (ν_{NO}) cm^{-1} (Et$_2$O). Absorption spectrum (THF) [nm, λ_{max} (M^{-1} cm^{-1}, ε)]: 285 (sh, 10 300), 380 (4900), 442 (sh, 2200), 634 (660). Anal. Calcd for $C_{36}H_{64}FeKN_4O_8Si_2$: C, 51.97; H, 7.75; N, 6.73. Found: C, 51.63; H, 7.48; N, 6.45. ^{15}N-labeled [(THF)$_2$-K-18-crown-6-ether][(^{15}NO)$_2$Fe(N(mesityl)(TMS))$_2$] was synthesized in the same manner by reaction of [(THF)$_2$-K-18-crown-6-ether][(^{15}NO)$_2$FeI$_2$] and [K][N(mesityl)(TMS)]. IR: 1674 s, 1622 s (ν_{15NO}) cm^{-1} (THF).

Synthesis of [(NO)$_2$Fe(N(mesityl)(TMS))$_2$] (5). Complex **4** (4.8812 g, 5.0 mmol) and [Cp$_2$Fe][BF$_4$] (1.3642 g, 5.0 mmol) were loaded into a Schlenk flask and dissolved in THF (30 mL) at −20 °C. After the mixture solution was stirred for 1 h at −20 °C, the deep-blue mixture solution was dried under vacuum. The residue was redissolved in the mixed diethyl ether and hexane (20:20 mL) at −20 °C. The mixture solution was then filtered through Celite. After the filtrate was dried under vacuum, diethyl ether (10 mL, 0 °C) was transferred to the crude solid and cooled to −40 °C for 1 day to yield dark blue, crystalline [(NO)$_2$Fe(N(mesityl)(TMS))$_2$] (**5**) isolated under vacuum (yield 1.110 g, first crop). The mother solution was concentrated and cooled to give a second crop (yield 0.291 g). Total yield of complex **5** is 1.401 g (53%). ^{1}H NMR (500 MHz, d_8-toluene, 25 °C): δ 6.82 (4H, br s, mesitylene), 2.31 (18H, br s, 2,4,6-CH_3-mesitylene), 0.17 ppm (18H, br s, Si(CH_3)$_3$). IR: 1786 s, 1733 s (ν_{NO}) cm^{-1} (THF); 1789 s, 1736 s (ν_{NO}) cm^{-1} (Et$_2$O). Absorption spectrum (THF) [nm, λ_{max} (M^{-1} cm^{-1}, ε)]: 269 (sh, 10 100), 374 (5700), 624 (7900), 664 (sh, 7700), 942 (620). Anal. Calcd for $C_{24}H_{40}FeN_4O_2Si_2$: C, 54.53; H, 7.63; N, 10.60. Found: C, 54.18; H, 7.62; N, 10.51. ^{15}N-labeled [(^{15}NO)$_2$Fe(N(mesityl)(TMS))$_2$] was synthesized in the same manner by reaction of [(THF)$_2$-K-18-crown-6-ether][(^{15}NO)$_2$Fe(N(mesityl)(TMS))$_2$] and [Cp$_2$Fe][BF$_4$]. IR: 1751 s, 1699 s (ν_{15NO}) cm^{-1} (THF). ^{15}N NMR (50.671 MHz, d_8-THF, 25 °C): δ 62.3 ppm (^{15}NO).

Reaction of complex 5, KC$_8$, and 18-crown-6-ether. Complex **5** (0.5282 g, 1.0 mmol), KC$_8$ (0.1487 g, 1.1 mmol), and 18-crown-6-ether (0.2642 g, 1.0 mmol) were loaded into a Schlenk flask and dissolved in THF (20 mL) at 0 °C. The reaction mixture was allowed to warm to ambient temperature and stirred for 1 h. After the resulting brown solution was filtered through Celite to remove the insoluble graphite, addition of diethyl ether and hexane to the mixture solution led to precipitation of the brown solid complex **4** (yield 0.851 g, 87%), characterized by IR spectroscopy.

Reaction of [PPN][(NO)$_2$Fe(SR)$_2$] (R = Ph, Et) and [Cp$_2$Fe][BF$_4$]. [PPN][(NO)$_2$Fe(SPh)$_2$] (0.1746 g, 0.2 mmol) (or [PPN][(NO)$_2$Fe(SEt)$_2$] (0.1554 g, 0.2 mmol)) and [Cp$_2$Fe][BF$_4$] (0.0546 g, 0.2 mmol) were loaded into a Schlenk flask and dissolved in THF−MeCN (5:5 mL). The reaction mixture was stirred for 30 min at room temperature and then dried under vacuum. The crude solid was redissolved in THF−diethyl ether (5:15 mL) and filtered through Celite to remove the insoluble solid [PPN][BF$_4$]. The filtrate was concentrated under vacuum, and then hexane was added to precipitate the known red-brown RRE [(NO)$_2$Fe(μ-SPh)]$_2$ (yield 0.039 g, 86%) (or the filtrate was dried under vacuum and then recrystallized from MeOH at −20 °C to obtain [(NO)$_2$Fe(μ-SEt)]$_2$ (yield 0.013 g, 36%)), characterized by IR and UV−vis (Supporting Information Scheme S1). The relatively low yield of [(NO)$_2$Fe(μ-SEt)]$_2$ resulting from oxidation of [PPN][(NO)$_2$Fe(SEt)$_2$] is attributed to the high solubility of [(NO)$_2$Fe(μ-SEt)]$_2$ in MeOH. The byproducts (PhS)$_2$ and [Cp$_2$Fe] existing in the THF−hexane solution were identified by ^{1}H NMR.

Magnetic Measurements. Magnetic data were recorded on a SQUID magnetometer (SQUID-VSM Quantum Design Co.) under a 0.5 T external magnetic field in the temperature range 2−300 K. Magnetic susceptibility data were corrected with ligands' diamagnetism by the tabulated Pascal's constants.

Magnetic Susceptibility. The temperature-independent magnetic susceptibility of complex **4** is shown in Supporting Information Figure S5a. The χ_M value increases from 1.539×10^{-3} cm^3 mol^{-1} at 300 K to a maximum of 94.665×10^{-3} cm^3 mol^{-1} at 2 K. The effective magnetic moment values decrease from 1.924 μ_B at 300 K to 1.714 μ_B at 2 K (Supporting Information Figure S5b). The corresponding $\chi_M T$ (0.463 cm^3 K mol^{-1}) and μ_{eff} (1.924 μ_B) values are near the spin-only values ($\chi_M T$ = 0.375 cm^3 K mol^{-1} and μ_{eff} = 1.732 μ_B) for the S = 1/2 system. The magnetic ground state is the result of strong antiferromagnetic coupling between high-spin Fe(III) (S_{Fe} = 5/2) and two nitroxyls (S_{NO} = 2). Assuming an energetically well-isolated magnetic ground state with total spin S_{tot} = 1/2, the Curie law fitting of the $\chi_M T$ vs T plot can be conducted by adopting g = 2.049, θ = −0.146 ± 0.005 K, and TIP = (226 ± 1.3) × 10^{-6} cm^3 mol^{-1} with R^2 = 0.993 (Supporting Information Figure S5c).

The magnetic susceptibility values of a powder sample of complex **5** increase from 1.612×10^{-4} cm^3 mol^{-1} at 300 K to 2.658×10^{-3} cm^3 mol^{-1} at 5 K (Supporting Information Figure S11a). The effective magnetic moment values decrease from 0.622 μ_B at 300 K to 0.326 μ_B at 5 K (Supporting Information Figure S11b). The corresponding $\chi_M T$ values decrease from 4.84×10^{-2} cm^3 K mol^{-1} at 300 K to 1.33×10^{-2} cm^3 K mol^{-1} at 5 K. Single-crystal X-ray diffraction, IR, and XAS suggest that the electronic structure of complex **5** is best described as [{Fe(NO)$_2$}^{9}−(L)$_2$$^{-\bullet}$] (L$^-$ = [N(mesityl)(TMS)]$^-$, L$^\bullet$ = aminyl radical). The Bleaney and Bowers equation $\chi_M = (2Ng^2\beta^2/kT)/[3 + \exp(\Delta_{S/T}/kT)]$, where $\Delta_{S/T}$ is the singlet/triplet (S/T) energy splitting ($\Delta_{S/T} = E_{S=1} - E_{S=0}$),[15] describes the covalent delocalization between aminyl radical and the {Fe(NO)$_2$}^{9} motif, leading to the ground state S = 0. In order to get the best fit of the SQUID data, the Hamiltonian ($\hat{H} = 2g\beta\hat{S}H$) was used to describe two uncoupled S = 1/2 radicals (spin-only value $\chi_M T$ = 0.75 cm^3 K mol^{-1}).[21] As shown below, fitting of the magnetic data is based on the assumption of the presence of [{Fe(NO)$_2$}^{9}−(L)$_2$$^{-\bullet}$] and uncoupled S = 1/2 diradicals (or decomposition species)

$$\chi_M^{exp} = (1 - p)\chi_M[\mathrm{Fe(NO)_2{-}(L)_2^{-\bullet}}] + p\chi_M(\text{uncoupled } S = 1/2 \text{ diradicals}) + \mathrm{TIP}$$

The best fit of the experimental data to the resonance hybrid model gives g({Fe(NO)$_2$}^{9}) = 2.015, g(L$^\bullet$) = 2.000, $\Delta_{S/T}$ = 1840 ± 68 cm^{-1}, θ = −4.45 ± 0.06 K, p = 3.19%, and TIP = (81.8 ± 0.4) × 10^{-6} cm^3 mol^{-1} with R^2 = 0.999 (Supporting Information Figure S11c). This result implicates that the electronic structure of complex **5** is best described as [{Fe(NO)$_2$}^{9}−(L)$_2$$^{-\bullet}$].

dx.doi.org/10.1021/ic302537d | Inorg. Chem. 2013, 52, 1631−1639

EPR Measurement. EPR measurements were performed at the X-band using a Bruker E580 spectrometer equipped with a Bruker ELEXSYS super-high-sensitivity cavity. X-band EPR spectra of THF solution of complex **2** (**3** and **4**) in a 4 mm EPR tube at 298 K were obtained with a microwave power of 5.972 mW (15.000 and 5.972 mW for **3** and **4**, respectively), frequency at 9.6556 GHz (9.6568 and 9.6555 GHz for **3** and **4**, respectively), conversion time of 20.39 ms, receiver gain of 20 (20 and 15 for **3** and **4**, respectively), and modulation amplitude of 0.8 G (0.8 and 0.1 G for **3** and **4**, respectively) at 100 kHz. X-Band EPR spectra of THF solution of complex **2** (**3** and **4**) in a 2 mm EPR tube at 77 K were obtained with a microwave power of 15.000 mW, frequency at 9.6568 GHz (9.6526 and 9.6519 GHz for **3** and **4**, respectively), conversion time of 81.79 ms (20.39 and 20.39 ms for **3** and **4**, respectively), receiver gain of 20, and modulation amplitude of 0.8 G at 100 kHz. EPR spectra were simulated by the program WINEPR (http://www.bruker-biospin.com/winepr.html).

X-ray Absorption Measurements. All X-ray absorption experiments were carried out at the National Synchrotron Radiation Research Center (NSRRC), Hsinchu, Taiwan. Fe K-edge spectra were recorded at room temperature. Data were averaged, and a smooth background was removed from all spectra by fitting a straight line to the pre-edge region and subtracting this straight line from the entire spectrum. Normalization of the data was accomplished by fitting a flat polynomial to the postregion and normalizing the edge jump to 1.0 at 7400 eV. For Fe K-edge measurements, experiments were performed in transmission mode at the BL17C wiggler beamline with a double-crystal Si(111) monochromator. Energy resolution $\Delta E/E$ was estimated to be about 2×10^{-4}. High harmonics were rejected by Rh-coated mirrors. Spectra were scanned from 6.912 to 7.972 keV. A reference Fe foil is always measured simultaneously, in which the first inflection point at 7112.0 eV of the Fe foil spectrum is used for energy calibration. Ion chambers used to measure the incident (I_0) and transmitted (I) beam intensities were filled with a mixture of N_2 and He gases and a mixture of N_2 and Ar gases, respectively.

Crystallography. Crystals of complexes **2**, **3**, **4**, and **5** chosen for X-ray diffraction study were measured in size 0.62 × 0.35 × 0.06, 076 × 0.54 × 0.04, 0.25 × 0.20 × 0.11, and 0.66 × 0.57 × 0.50 mm, respectively. Crystals were mounted on a glass fiber. Unit-cell parameters were obtained by least-squares refinement. Diffraction measurements for complexes **2**, **3**, **4**, and **5** were carried out on a Bruker Kappa Apex II diffractometer with graphite-monochromated Mo Kα radiation (λ = 0.7107 Å) and between 1.44° and 25.04° for **2** (1.04° and 25.03° for **3**, 1.70° and 25.00° for **4**, 1.87° and 25.03° for **5**, respectively). Least-squares refinement of the positional and anisotropic thermal parameters of all non-hydrogen atoms and fixed hydrogen atoms was based on F^2. The SHELXTL structure refinement program was employed.[22] Two THF were squeezed in complex **2** due to large disorder. Summary of crystal data, intensity collection, and structure refinement parameters for complexes **2**, **3**, **4**, and **5** are shown in Supporting Information Table S4.

Molecular Orbital Calculation. All MO (molecular orbitals) and TD-DFT (time-dependent-density functional theory) calculations were performed on the ORCA electronic structure package version 2.8.0.[23] Coordinates used for geometry optimization of complexes **4** and **5** were based on the experimental structures taken from the X-ray diffraction experiments. The coordinate system employed is such that the origin is set at the Fe atom, the x axis bisects the angle ∠N(O)−Fe−N(O), and the y axis is perpendicular to the plane of N(O)−Fe−N(O). In order to find a suitable exchange functional to describe the electronic structure in such complexes, the different mixing ratio of Hartree−Fock exchange (HFx) contributions were examined. The BP86,[24] B3LYP (HFx = 20%),[25] B3LYP* (HFx = 15%),[26] and O3LYP (HFx = 11.61%)[27] exchange functionals with the all-electron def2-TZVP(-f) basis set on Fe, Si, N, O, C, and H atoms were used in geometry optimization. ZORA was used to account for the relativistic effect. Both structures were optimized in an unrestricted open shell with C_1 symmetry, and there was no imaginary frequency observed. In comparison with the experimental magnetic measurements, the B3LYP* functional was more suitable in these two molecules. Löwdin population analysis was used to obtain the contributions of Fe, NO, and N (NR_2 ligand) on each MO. Isosurface plots of the MOs were generated using the Molekel program with an isovalue surface at 0.04 au.[28]

The effects of different exchange functionals are list in Supporting Information Table S2. The results indicate that the total energy differences of B3LYP* (∼1460 cm^{-1}) between the triplet and the singlet is the closest to the magnetic measurement (∼1840 cm^{-1}). The corresponding IR vibrational frequencies of NO are also shown in Supporting Information Table S3. Frontier MO energy diagrams of complexes **4** and **5** are depicted in Supporting Information Figures S12 and S13, respectively. In each MO, the corresponding contributions of Fe 3d, NO 2p, and N (NR_2 ligand) 2p orbitals are listed. On the basis of previous reports by Su et al.,[5e,29] there are four unoccupied α orbitals 142−145 derived from NO π^* orbitals and five unoccupied β orbitals 141−145 dominant from the 3d character of Fe in the MOs of DNIC **4**. This implies that the Fe 3d orbitals have five α electrons and the NO π^* orbitals have four β electrons, which signifies the electronic structure $\{Fe^{III}(NO^-)_2\}^9$ for DNIC **4**. Composition analysis of MO of DNIC **5** also indicates the $\{Fe^{III}(NO^-)_2\}^9$ electronic configuration, that is, oxidation from DNIC **4** to **5** can be characterized as removing one electron from [N(mesityl)(TMS)]-coordinate ligands. TD-DFT calculation on the UV−vis−NIR region of complex **5** is displayed in Figure 7. The transition around 942 nm is assigned as the transition from the HOMO (MO140) to the LUMO (MO141). The HOMO was mainly contributed from the N(aminyl ligands) (Fe $3d_{xy} \approx 5.2\%$, NO ≈ 17.8%, and $N_{(NR2)} \approx 30.9\%$), and the LUMO is mainly made up of the Fe site (Fe $3d_{x2-y2} \approx 38.4\%$, NO ≈ 20.6%, and $N_{(NR2)} \approx 18.2\%$), implicating charge transfer occurs from aminyl ligands to the Fe site.

■ ASSOCIATED CONTENT

Ⓢ Supporting Information

EPR, SQUID, $^1H/^{15}N$ NMR, UV−vis, CV, and XAS experiments and crystallographic and computational details. This material is available free of charge via the Internet at http://pubs.acs.org.

■ AUTHOR INFORMATION

Corresponding Author

*E-mail: wfliaw@mx.nthu.edu.tw; ijuihsu@ntut.edu.tw.

Notes

The authors declare no competing financial interest.

■ ACKNOWLEDGMENTS

We gratefully acknowledge financial support from the National Science Council of Taiwan. We also thank the National Synchrotron Radiation Research Center, Taiwan (NSRRC), and National Center for High-Performance Computing (NCHC) for their support on the hardware and software applied in this work. The authors thank Dr. Jyh-Fu Lee for XAS experiments and Mr. Ting-Shen Kuo for single-crystal X-ray structural determinations.

■ REFERENCES

(1) (a) Butler, A. R.; Megson, I. L. *Chem. Rev.* **2002**, *102*, 1155−1165. (b) Vanin, A. F. *Nitric Oxide* **2009**, *21*, 1−13. (c) Tonzetich, Z. J.; McQuade, L. E.; Lippard, S. J. *Inorg. Chem.* **2010**, *49*, 6338−6348. (d) Smith, L. J.; Stapleton, M. R.; Fullstone, G. J.; Crack, J. C.; Thomson, A. J.; Le Brun, N. E.; Hunt, D. M.; Harvey, E.; Adinolfi, S.; Buxton, R. S.; Green, J. *Biochem. J.* **2010**, *432*, 417−427. (e) Lewandowska, H.; Kalinowska, M.; Brzoska, K.; Wojciuk, K.; Wojciuk, G.; Kruszewski, M. *Dalton Trans.* **2011**, *40*, 8273−8289.

(2) (a) Tsou, C.-C.; Liaw, W.-F. *Chem.—Eur. J.* **2011**, *17*, 13358−13366. (b) Lu, T.-T.; Chen, C.-H.; Liaw, W.-F. *Chem.—Eur. J.* **2010**, *16*, 8088−8095. (c) Tsai, F.-T.; Kuo, T.-S.; Liaw, W.-F. *J. Am. Chem. Soc.* **2009**, *131*, 3426−3427. (d) Tsai, F.-T.; Chen, P.-L.; Liaw, W.-F. *J.*

Am. Chem. Soc. **2010**, *132*, 5290−5299. (e) Tran, N. G.; Kalyvas, H.; Skodje, K. M.; Hayashi, T.; Moenne-Loccoz, P.; Callan, P. E.; Shearer, J.; Kirschenbaum, L. J.; Kim, E. *J. Am. Chem. Soc.* **2011**, *133*, 1184−1187.

(3) Enemark, J. H.; Feltham, R. D. *Coord. Chem. Rev.* **1974**, *13*, 339−406.

(4) (a) Atkinson, F. L.; Blackwell, H. E.; Brown, N. C.; Connelly, N. G.; Crossley, J. G.; Orpen, A. G.; Rieger, A. L.; Rieger, P. H. *J. Chem. Soc., Dalton Trans.* **1996**, 3491−3502. (b) Reginato, N.; McCrory, C. T. C.; Pervitsky, D.; Li, L. *J. Am. Chem. Soc.* **1999**, *121*, 10217−10218. (c) Hung, M.-C.; Tsai, M.-C.; Liaw, W.-F. *Inorg. Chem.* **2006**, *45*, 6041−6047. (d) Tonzetich, Z. J.; Do, L. H.; Lippard, S. J. *J. Am. Chem. Soc.* **2009**, *131*, 7964−7965. (e) Wang, J.-H.; Chen, C.-H. *Inorg. Chem.* **2010**, *49*, 7644−7646. (f) Hess, J. L.; Hsieh, C. H.; Reibenspies, J. H.; Darensbourg, M. Y. *Inorg. Chem.* **2011**, *50*, 8541−8552.

(5) (a) Jaworska, M.; Stasicka, Z. *J. Organomet. Chem.* **2004**, *689*, 1702−1713. (b) Tsai, M.-C.; Tsai, F.-T.; Lu, T.-T.; Tsai, M.-L.; Wei, Y.-C.; Hsu, I.-J.; Lee, J.-F.; Liaw, W.-F. *Inorg. Chem.* **2009**, *48*, 9579−9591. (c) Hopmann, K. H.; Conradie, J.; Ghosh, A. *J. Phys. Chem. B* **2009**, *113*, 10540−10547. (d) Ye, S.; Neese, F. *J. Am. Chem. Soc.* **2010**, *132*, 3646−3647. (e) Lu, T.-T.; Lai, S.-H.; Li, Y.-W.; Hsu, I.-J.; Jang, L.-Y.; Lee, J.-F.; Chen, I.-C.; Liaw, W.-F. *Inorg. Chem.* **2011**, *50*, 5396−5406. (f) Yeh, S.-W.; Lin, C.-W.; Li, Y.-W.; Hsu, I.-J.; Chen, C.-H.; Jang, L.-Y.; Lee, J.-F.; Liaw, W.-F. *Inorg. Chem.* **2012**, *51*, 4076−4087.

(6) (a) Lorković, I. M.; Ford, P. C. *J. Am. Chem. Soc.* **2000**, *122*, 6516−6517. (b) Conradie, J.; Wondimagegn, T.; Ghosh, A. *J. Am. Chem. Soc.* **2003**, *125*, 4968−4969. (c) Patterson, J. C.; Lorković, I. M.; Ford, P. C. *Inorg. Chem.* **2003**, *42*, 4902−4908. (d) Wang, J.; Schopfer, M. P.; Puiu, S. C.; Sarjeant, A. A.; Karlin, K. D. *Inorg. Chem.* **2010**, *49*, 1404−1419.

(7) Roncaroli, F.; van Eldik, R.; Olabe, J. A. *Inorg. Chem.* **2005**, *44*, 2781−2790.

(8) Lu, T.-T.; Chiou, S.-J.; Chen, C.-Y.; Liaw, W.-F. *Inorg. Chem.* **2006**, *45*, 8799−8806.

(9) (a) D'Autréaux, B.; Horner, O.; Oddou, J.-L.; Jeandey, C.; Gambarelli, S.; Berthomieu, C.; Latour, J.-M.; Michaud-Soret, I. *J. Am. Chem. Soc.* **2004**, *126*, 6005−6016. (b) Lin, Z.-S.; Lo, F.-C.; Li, C.-H.; Chen, C.-H.; Huang, W.-N.; Hsu, I.-J.; Lee, J.-F.; Horng, J.-C.; Liaw, W.-F. *Inorg. Chem.* **2011**, *50*, 10417−10431.

(10) (a) Büttner, T.; Geier, J.; Frison, G.; Harmer, J.; Calle, C.; Schweiger, A.; Schönberg, H.; Grützmacher, H. *Science* **2005**, *307*, 235−238. (b) Maire, P.; Königsmann, M.; Sreekanth, A.; Harmer, J.; Schweiger, A.; Grützmacher, H. *J. Am. Chem. Soc.* **2006**, *128*, 6578−6580. (c) Königsmann, M.; Donati, N.; Stein, D.; Scho:nberg, H.; Harmer, J.; Sreekanth, A.; Grützmacher, H. *Angew. Chem., Int. Ed. Engl.* **2007**, *46*, 3567−3570. (d) Miyazato, Y.; Wada, T.; Muckerman, J. T.; Fujita, E.; Tanaka, K. *Angew. Chem., Int. Ed. Engl.* **2007**, *46*, 5728−5730. (e) Adhikari, D.; Mossin, S.; Basuli, F.; Huffman, J. C.; Szilagyi, R. K.; Meyer, K.; Mindiola, D. J. *J. Am. Chem. Soc.* **2008**, *130*, 3676−3682. (f) Hicks, R. G. *Angew. Chem., Int. Ed. Engl.* **2008**, *47*, 7393−7395. (g) Mankad, N. P.; Antholine, W. E.; Szilagyi, R. K.; Peters, J. C. *J. Am. Chem. Soc.* **2009**, *131*, 3878−3880.

(11) Huang, H.-W.; Tsou, C.-C.; Kuo, T.-S.; Liaw, W.-F. *Inorg. Chem.* **2008**, *47*, 2196−2204.

(12) (a) Harrop, T. C.; Song, D.; Lippard, S. J. *J. Am. Chem. Soc.* **2006**, *126*, 3528−3529. (b) Tsai, M.-L.; Liaw, W.-F. *Inorg. Chem.* **2006**, *45*, 6583−6585. (c) Tsou, C.-C.; Lu, T.-T.; Liaw, W.-F. *J. Am. Chem. Soc.* **2007**, *129*, 12626−12627. (d) Shih, W.-C.; Lu, T.-T.; Yang, L.-B.; Tsai, F.-T.; Chiang, M.-H.; Lee, J.-F.; Chiang, Y.-W.; Liaw, W.-F. *J. Inorg. Biochem.* **2012**, *113*, 83−93.

(13) (a) Butler, A. R.; Glidewell, C.; Hyde, A. R.; McGinnis, J. *Inorg. Chem.* **1985**, *24*, 2931−2934. (b) Glidewell, C.; Johnson, I. L. *Chem. Scr.* **1987**, *27*, 441−444. (c) Mason, J.; Larkworthy, L. F.; Moore, E. A. *Chem. Rev.* **2002**, *102*, 913−934.

(14) Tang, Y.; Zakharov, L. N.; Rheingold, A. L.; Kemp, R. A. *Organometallics* **2005**, *24*, 836−841.

(15) Chen, P.; Root, D. E.; Campochiaro, C.; Fujisawa, K.; Solomon, E. I. *J. Am. Chem. Soc.* **2003**, *125*, 466−474.

(16) Tonzetich, Z. J.; Wang, H.; Mitra, D.; Tinberg, C. E.; Do, L. H.; Jenney, F. E., Jr.; Adams, M. W.; Cramer, S. P.; Lippard, S. J. *J. Am. Chem. Soc.* **2010**, *132*, 6914−6916.

(17) (a) Yang, J.; Duan, X.; Landry, A. P.; Ding, H. *Free Radic. Biol. Med.* **2010**, *49*, 268−274. (b) Hickok, J. R.; Sahni, S.; Shen, H.; Arvind, A.; Antoniou, C.; Fung, L. W.; Thomas, D. D. *Free Radical Biol. Med.* **2011**, *51*, 1558−1566. (c) Suryo Rahmanto, Y.; Kalinowski, D. S.; Lane, D. J.; Lok, H. C.; Richardson, V.; Richardson, D. R. *J. Biol. Chem.* **2012**, *287*, 6960−6968.

(18) (a) Hayton, T. W.; McNeil, W. S.; Patrick, B. O.; Legzdins, P. *J. Am. Chem. Soc.* **2003**, *125*, 12935−12944. (b) Hsieh, C.-H.; Darensbourg, M. Y. *J. Am. Chem. Soc.* **2010**, *132*, 14118−14125. (c) Hauser, C.; Glaser, T.; Bill, E.; Weyhermüller, T.; Wieghardt, K. *J. Am. Chem. Soc.* **2000**, *122*, 4352−4365. (d) Serres, R. G.; Grapperhaus, C. A.; Bothe, E.; Bill, E.; Weyhermüller, T.; Neese, F.; Wieghardt, K. *J. Am. Chem. Soc.* **2004**, *126*, 5138−5153. (e) Patra, A. K.; Dube, K. S.; Sanders, B. C.; Papaefthymiou, G. C.; Conradie, J.; Ghosh, A.; Harrop, T. C. *Chem. Sci.* **2012**, *3*, 364−369. (f) Hayton, T. W.; McNeil, W. S.; Patrick, B. O.; Legzdins, P. *J. Am. Chem. Soc.* **2003**, *125*, 12935−12944.

(19) Mcbride, D. W.; Stafford, S. L.; Stone, F. G. A. *Inorg. Chem.* **1962**, *1*, 386−388.

(20) Connelly, N. G.; Gardner, C. *J. Chem. Soc., Dalton Trans.* **1976**, 1525−1527.

(21) Kahn, O. *Molecular Magnetism*; VCH Publishers: New York, 1993; pp 103−107.

(22) Sheldrick, G. M. *SHELXTL, A Program for Crystal Structure Determination*; Siemens Analytical X-ray Instruments, Inc.: Madison, WI, 1994.

(23) Neese, F. *ORCA-an ab Initio, Density functional and Semi-empirical Electronic Structure Package*, version 2.8.0; University of Bonn: Germany, 2010.

(24) (a) Perdew, J. P.; Yang, W. *Phys. Rev. B* **1986**, *33*, 8800−8802. (b) Becke, A. D. *Phys. Rev. A* **1988**, *38*, 3098−3100.

(25) Stephens, P. J.; Devlin, F. J.; Chabalowski, C. F.; Frisch, M. J. *J. Phys. Chem.* **1994**, *98*, 11623−11627.

(26) Reiher, M.; Salomon, O.; Hess, B. A. *Theor. Chem. Acc.* **2001**, *107*, 48−55.

(27) Cohen, A. J.; Handy, N. C. *Mol. Phys.* **2001**, *99*, 607−615.

(28) Flükiger, P.; Lüthi, H. P.; Portmann, S.; Weber, J. *MOLEKEL 4.3*; Swiss Center for Scientific Computing: Manno, Switzerland, 2000−2002.

(29) Sun, N.; Liu, L. V.; Dey, A.; Villar-Acevedo, G.; Kovacs, J. A.; Darensbourg, M. Y.; Hodgson, K. O.; Hedman, B.; Solomon, E. I. *Inorg. Chem.* **2011**, *50*, 427−436.